T-HuDe: Through-The-Wall Human Detection with WiFi Devices

Wei Zeng(✉), Zengshan Tian, Yue Jin, and Xi Chen

Chongqing Key Lab of Mobile Communications Technology,
School of Communication and Information Engineering,
Chongqing University of Posts and Telecommunications, Chongqing, China
zengweicq@gmail.com, tianzs@cqupt.edu.cn, jinyue063@gmail.com,
chenxiopr@gmail.com

Abstract. With the rapid development of emerging smart homes applications, the home security systems based on passive detection without carrying any devices has been increasing attention in recent years. Through-The-Wall (TTW) detection is a great challenge since through-the-wall signal can be severely attenuated, and some of the existing TTW-based detection techniques require special equipment or have strict restrictions on placement of devices. Due to the near-ubiquitous wireless coverage, WiFi based passively human detection technique becomes a good solution. In this paper, we propose a robust scheme for device-free Through-the-wall Human Detection (T-HuDe) in TTW with Channel State Information (CSI), which can provide more fine-grained movement information. Especially, T-HuDe utilizes motion information on WiFi signal and uses statistical information of motion characteristics as parameters. To evaluate T-HuDe performance, we prototype it in different environments with commodity devices, and the test results show that human activity detection rate and human absence detection rate of T-HuDe are both above 93% in most detection areas.

Keywords: Through-The-Wall · Active human detection · Channel State Information

1 Introduction

With the rapid development of applications such as smart homes, indoor-based motion detection has recently gained more attention. In order to make a better interactive experience for humans and smart homes, more and more researchers

This work is supported in part by National Natural Science Foundation of China (61771083, 61704015), the Program for Changjiang Scholars and Innovative Research Team in University (IRT1299), Special Fund of Chongqing Key Laboratory (CSTC), Fundamental and Frontier Research Project of Chongqing (cstc2017jcyjAX0380), and University Outstanding Achievement Transformation Project of Chongqing (KJZH17117).

H. Gao et al. (Eds.): ChinaCom 2019, LNICST 313, pp. 192–204, 2020.
https://doi.org/10.1007/978-3-030-41117-6_16

have tapped into device-free sensing, which does not require the target to carry any device. Currently, there are many device-free sensing technologies, such as camera-based, infrared-based, etc. Camera-based motion detection systems have issues of individual privacy, and people behind the wall cannot be detected. Infrared-based motion detection technology has the disadvantage of requiring special equipment support which limits its application scenarios. At the same time, WiFi-based passive human detection can effectively avoid the above disadvantages due to the widely available WiFi signals interacting with objects in the environment.

Recently, using WiFi signals to passively sense the human activity has developed rapidly, including indoor localization [1,2], recognition [3–5], heartbeat detection [6,7], etc. On the one hand, the improvement of technologies such as Orthogonal Frequency Division Multiplexing (OFDM) and Multiple-Input-Multiple-Output (MIMO) enables systems to obtain more fine-grained data using fewer devices. On the other hand, it does not require users to carry any equipment, which is suitable for application of smart home.

Before implementing applications such as device-free passively localization, it is necessary to use device-free sensing technologies to detect whether there are any people in the area of interests without attaching any device [8]. However, there is a wall between the receiver and the transmitter in the home security system, and the TTW signal will be seriously attenuated. Existing techniques that extract statistical features directly from the data, such as PADs [10] and SIED [11], etc., are difficult to apply to complex indoor environments.

In this paper, we leverage Channel State Information (CSI) data between three antennas of the receiver WiFi Network Interface Cards (NIC) to implement device-free Through-the-wall Human Detection (T-HuDe). Our contribution is to use statistical information of motion characteristics, to robustly detect human movement in TTW scenario. Meanwhile, we use Support Vector Machine [13] to detect the active human behind the wall, and test results show that human activity detection rate and human absence detection rate of T-HuDe are both above 93% in most detection areas.

2 Preliminaries

2.1 Channel State Information

Leveraging the off-the-shelf NIC with slight driver modification, $N = 30$ orthogonal subcarrier data can be exported from the CSI data. Taking multipath propagation into consideration, the wireless channel of single carrier can be described as:

$$H(f) = \sum_{m=1}^{M} \alpha_m e^{-j2\pi f \tau_m} \tag{1}$$

where $H(f)$ is a subcarrier with a center frequency of f, and M is the total number of multipath of subcarrier, α_m and τ_m are the complex attenuation and propagation delay for the mth signal path, respectively.

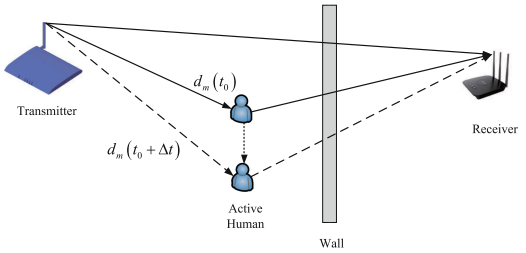

Fig. 1. Reflection path changed by active human.

When there is no object movement the wireless channel in indoor environment is relatively stable, yet it is caused large fluctuation on amplitude and phase of subcarriers that moving human intersect or walk around the transceiver link. Meanwhile, Doppler Frequency Shift (DFS) induced by human movement can introduce additional phase, which can be a key indicator for movement detection.

2.2 Doppler Frequency Shift

The signal is transmitted from the transmitter and experiences through several different paths back to the receiver, and the received signal is a superposition of these different path signals. We can use this multipath components to jointly estimate the DFS [12]. As illustrated in Fig. 1, the path length of the reflection signal changes as the human moves, and produces the DFS. The DFS is given by:

$$f_D = \frac{1}{\lambda} \frac{d_m(t_0 + \Delta t) - d_m(t_0)}{\Delta t} \tag{2}$$

where f_D is the Doppler frequency shift during time Δt, $d_m(t_0)$ is the path length of the human reflection signal at time t_0, λ is the carrier wavelength of the signal.

Active human in the indoor environment will produce DFS, which is difficult to use directly since TTW signal will be severely attenuated. However, we can calculate the trend of the spectrum power corresponding to the DFS of TTW signal, which can well describe the variance of DFS and further describe the changes of human induced channel.

3 Methodology

In this section, we illustrate the design of T-HuDe by real measurements.

3.1 Antenna Selection

The number of antennas on the device increases with the development of MIMO technology. However, different antennas on the same device exhibit different

performance, as shown in Fig. 2. Figure 2(a) shows the difference term of the amplitude of each subcarrier of the three antennas, Fig. 2(b) shows the distribution of the amplitude of each subcarrier of the three antennas. The larger the standard deviation, the more likely received signal on an antenna is more sensitive to human movement [15]. Therefore, the strategy for selecting antennas is as follows:

$$ant\_opt = \underset{ant=\{1,2,3\}}{\arg\max} \left\{ \frac{1}{N} \sum_{i \in N} \text{std}\left(|H\left(f_i\right)| \right) \right\} \tag{3}$$

where N is the number of subcarriers, and ant is the serial number of the antenna. We consider the variation of all subcarrier data in one antenna, calculate the standard deviation of all subcarrier variations, and the antenna with the largest average standard deviation is the selected antenna.

3.2 Phase Sanitizations

The phase of CSI can be mined some useful characteristics to determine whether there is an active person in the current environment. However, the raw phase has severe random noise, and it is necessary to eliminate the random noise before using the phase information. Combined with the phase information induced by active human, CSI is described by:

$$\begin{aligned} H\left(f\right) &= e^{-j2\pi\delta} \sum_{m=1}^{M} \alpha_m e^{-j2\pi f\left(\tau_m + \frac{d_m(t_0+\Delta t)-d_m(t_0)}{c}\right)} \\ &= e^{-j2\pi\delta} \sum_{m=1}^{M} \beta_m e^{-j2\pi f \frac{d_m(t_0+\Delta t)-d_m(t_0)}{c}} \end{aligned} \tag{4}$$

where $\beta_m = \alpha_m e^{-j2\pi f \tau_m}$, δ is random phase offset, c is the propagation speed of the CSI signal in the air. As illustrated in Fig. 1, the signal propagation paths from the transmitter to the receiver can be divided into two categories: some signal propagation paths do not change over time and remain constant, which called static paths; some signal propagation paths change over time, which called dynamic path [14]. Equation (4) can be rewritten as:

$$H\left(f\right) = e^{-j2\pi\delta} \left(H_S\left(f\right) + \sum_{m \in P_d} \beta_m e^{-j2\pi f \frac{d_m(t_0+\Delta t)-d_m(t_0)}{c}} \right) \tag{5}$$

where $H_S(f)$ is vector sum of static paths, P_d is the set of dynamic paths. The distortion phase produced by δ can lead to wrong DFS being estimated. To avoid this phenomenon, we adopt conjugate multiplication to eliminate phase offset.

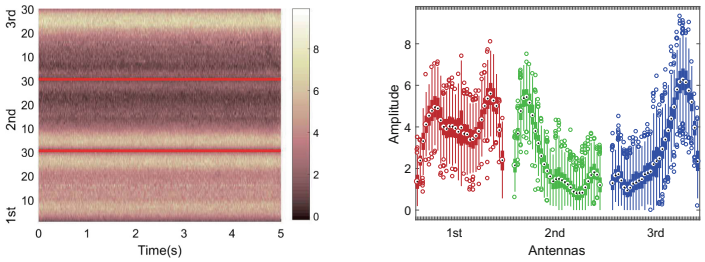

(a) The difference term of different antenna amplitude (b) The distribution of different antenna amplitudes

Fig. 2. The amplitude in different antenna.

The conjugate multiplication of the antenna is as follows:

$$\begin{aligned} |H(f)|^2 &= H(f)\bar{H}(f) \\ &= |H_S(f)|^2 + H_S(f)\sum_{m\in P_d}\beta_m e^{j2\pi f\frac{d_m(t_0+\Delta t)-d_m(t_0)}{c}} \\ &+ \bar{H}_S(f)\sum_{m\in P_d}\beta_m e^{-j2\pi f\frac{d_m(t_0+\Delta t)-d_m(t_0)}{c}} \\ &+ \sum_{m_1\in P_d}\sum_{m_2\in P_d}\beta_{m_1}\beta_{m_2}e^{-j2\pi f\left(\frac{d_{m_1}(t_0+\Delta t)-d_{m_1}(t_0)}{c}-\frac{d_{m_2}(t_0+\Delta t)-d_{m_2}(t_0)}{c}\right)} \end{aligned} \tag{6}$$

We use conjugate multiplication to eliminate the phase offset, but the conjugate multiplied data contains other terms. The product terms among dynamic paths is small and can be ignored, and the value of the conjugate multiplication of static paths is large but regarded as constants in a short time. The product terms of interest are included in the conjugate multiplication of static paths and dynamic paths, which has same value and opposite directions of the DFS [12].

3.3 Filtering

From Eq. (6) we can see that the conjugate multiplication result of an antenna, also known as Channel Frequency Response (CFR) power, can be divided into four parts, of which only two parts contain useful information. The value of the conjugate multiplication of static paths occupies the dominant component and belongs to the zero-frequency component, and considering some low-frequency interference, the lower cutoff frequency of the bandpass filter is set to 2 Hz. Assuming that the speed of the active person is less than 2 m/s and filtering out high frequency components such as some burst noise, the higher cutoff frequency is set to 80 Hz [12].

After using the bandpass filter, a conjugate multiplied component of static paths and dynamic paths can be obtained. In Eq. (6), its component consists

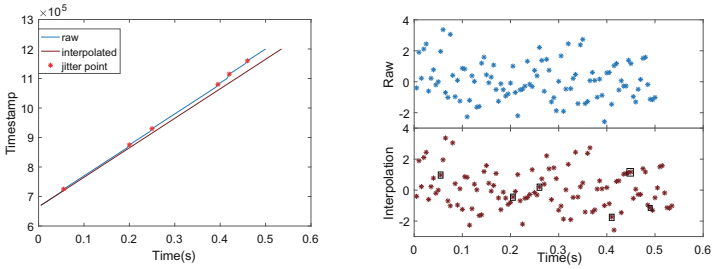

(a) Timestamp jitter

(b) Raw CFR power and interpolated CFR power

Fig. 3. Raw data and interpolated data.

of two parts, which can estimate two Doppler velocities of the same value but opposite directions, but this does not affect the estimation, because only the spectrum power corresponding to the Doppler velocity is concerned instead of the Doppler velocity direction. Based on the above discussion, the subsequent partial default Doppler velocity is positive.

3.4 Linear Interpolation

In general, timestamps are consecutive in adjacent packets. However, data loss is common in data collection and causes sample jitter, while timestamp discontinuities and data loss are related. Since each timestamp corresponds to a filtered CFR power value, we look for the jitter point of the timestamp and use linear interpolation for the corresponding filtered CFR power. As shown in Fig. 3, Fig. 3(a) is the jitter and interpolated timestamp, the timestamp is discrete, and for better description, we draw the timestamps as contiguous, Fig. 3(b) is the jittered and interpolated filtered CFR power. After interpolating the timestamp, a complete filtered CFR power sequence value can be obtained.

3.5 Active Human Detection

Estimated Spectrum Power. In commercial WiFi devices, WiFi signals are transmitted on multiple subcarriers. Countering the frequency selective fading that exists between carriers, we use the MUSIC-based Doppler estimation algorithm [12] with multi-carrier information.

For simplicity, assume that there are K consecutive CSI samples with a sampling interval of microseconds. At the same time, assume that the velocity of K samples is constant during time t_0 and the velocity is $v\left(t_0\right) = v\left(t_0 + \Delta t_k\right) = \frac{d(t_0+\Delta t_k)-d(t_0)}{\Delta t_k}$, where Δt_k is the time interval between the kth sample and the first sample at time t_0. If the path is a static path, $v(t_0)$ is zero, and the CSI phase does not change over time. On the contrary, $v(t_0)$ in the dynamic path is nonzero, and the CSI phase changes over time. If there is only a single signal path, the

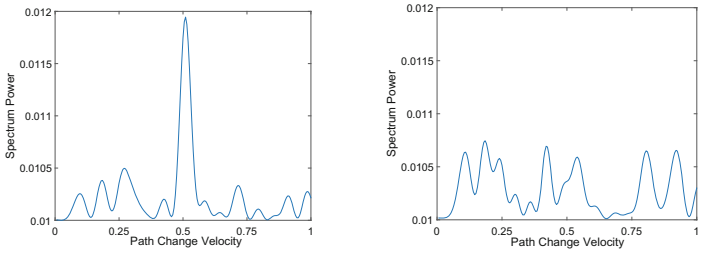

(a) Human Activity (b) Human Absence

Fig. 4. The spectrum power corresponding to path change velocity in TTW detection.

phase difference between time $t_0 + \Delta t_k$ and time t_0 is $p_{t_0}(\Delta t_k) = e^{-j2\pi f \frac{v(t_0)\Delta t_k}{c}}$, where f is the carrier frequency. Therefore, the phase difference of the K samples compared to the first sample is as follows:

$$\mathbf{s}(v_{t_0}) = \left[1\ p_{t_0}(\Delta t_2)\ p_{t_0}(\Delta t_3) \ldots p_{t_0}(\Delta t_k)\right]^T \tag{7}$$

The vector $\mathbf{s}(v_{t_0})$ is the steering vector. The received signal matrix composed of M multipath signals is as follows:

$$\begin{aligned}
\mathbf{X}(f) &= \left[H(f,t_0)\ H(f,t_0+\Delta t_2) \ldots H(f,t_0+\Delta t_K)\right]^T \\
&= \begin{bmatrix} 1 & 1 & \ldots & 1 \\ p_{t_0,1}(\Delta t_2) & p_{t_0,2}(\Delta t_2) & \ldots & p_{t_0,M}(\Delta t_2) \\ \vdots & \vdots & \ddots & \vdots \\ p_{t_0,1}(\Delta t_K) & p_{t_0,2}(\Delta t_K) & \ldots & p_{t_0,M}(\Delta t_K) \end{bmatrix} \begin{bmatrix} \beta_1 \\ \beta_2 \\ \vdots \\ \beta_M \end{bmatrix} + \mathbf{N}(f) \\
&= \left[\mathbf{s}(v_{t_0,1})\ \mathbf{s}(v_{t_0,2}) \ldots \mathbf{s}(v_{t_0,M})\right]\mathbf{c} + \mathbf{N}(f) \\
&= \mathbf{Sc} + \mathbf{N}(f)
\end{aligned} \tag{8}$$

where $p_{t_0,m}(\Delta t_k)$ is the phase difference of the mth path time $t_0 + \Delta t_k$ and time t_0, $\mathbf{s}(v_{t_0,m})$ is the steering vector of the mth path, $\mathbf{N}(f)$ is noise matrix, and $\mathbf{c} = \left[\beta_1\ \beta_2 \ldots \beta_M\right]^T$ is a signal vector. The CSI data contains N subcarriers, and the received CSI data can be written as follows:

$$\begin{aligned}
\mathbf{Y}(f) &= \left[\mathbf{X}(f_1)\ \mathbf{X}(f_2) \ldots \mathbf{X}(f_N)\right] \\
&= \begin{bmatrix} 1 & 1 & \ldots & 1 \\ p_{t_0,1}(\Delta t_2) & p_{t_0,2}(\Delta t_2) & \ldots & p_{t_0,M}(\Delta t_2) \\ \vdots & \vdots & \ddots & \vdots \\ p_{t_0,1}(\Delta t_K) & p_{t_0,2}(\Delta t_K) & \ldots & p_{t_0,M}(\Delta t_K) \end{bmatrix} \begin{bmatrix} \beta_{1,f_1} & \beta_{1,f_2} & \ldots & \beta_{1,f_N} \\ \beta_{2,f_1} & \beta_{2,f_2} & \ldots & \beta_{2,f_N} \\ \vdots & \vdots & \ddots & \vdots \\ \beta_{M,f_1} & \beta_{M,f_2} & \ldots & \beta_{M,f_N} \end{bmatrix} + \mathbf{N}(f) \\
&= \left[\mathbf{s}(v_{t_0,1})\ \mathbf{s}(v_{t_0,2}) \ldots \mathbf{s}\left(v_{t_0,M}\right)\right]\left[\mathbf{c}(f_1)\ \mathbf{c}(f_2) \ldots \mathbf{c}(f_N)\right] + \mathbf{N}(f) \\
&= \mathbf{SC} + \mathbf{N}(f)
\end{aligned} \tag{9}$$

where $\mathbf{c}(f_n)$ is a vector with carrier frequency f_n, $\mathbf{C} = \left[\mathbf{c}(f_1)\ \mathbf{c}(f_2) \ldots \mathbf{c}(f_N)\right]$ is the signal matrix. To estimate the steering vector $\mathbf{s}(v_{t_0})$ containing DFS

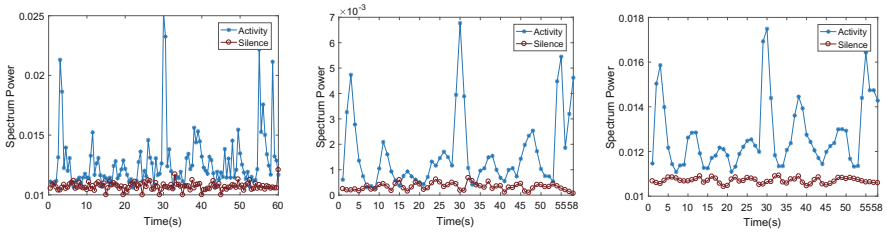

(a) The spectrum power of raw data (b) The mean of the first-order difference of the spectrum power (c) The mean of the spectrum power

Fig. 5. Activity and silence spectrum power.

information, the MUSIC algorithm is applied to Eq. 9. The correlation matrix $\mathbf{R_{YY}}$ of the matrix Y is as follows:

$$\begin{aligned}\mathbf{R_{YY}} &= \mathrm{E}\left[\mathbf{Y}\mathbf{Y}^{\mathrm{H}}\right] \\ &= \mathbf{S}\mathrm{E}\left[\mathbf{C}\mathbf{C}^{\mathrm{H}}\right]\mathbf{S}^{\mathrm{H}} + \mathrm{E}\left[\mathbf{N}\mathbf{N}^{\mathrm{H}}\right] \\ &= \mathbf{S}\mathbf{R_{CC}}\mathbf{S}^{\mathrm{H}} + \sigma^2\mathbf{I}\end{aligned} \tag{10}$$

where $\mathbf{R_{CC}}$ is the correlation matrix of the signal matrix $\mathbf{C}$, σ^2 is the noise variance, and $\mathbf{I}$ is the unit matrix. While $\mathbf{R_{CC}}$ is a full rank matrix with K eigenvalues, including the smallest $K-L$ eigenvalues associated with noise, and the L eigenvalues associated with the signal. The ith eigenvalue corresponds to the eigenvector $\mathbf{e}_i$, the noise eigenvector and the signal eigenvector constitute a noise subspace $\mathbf{E}_N = \left[\mathbf{e}_1\ \mathbf{e}_2\ \ldots\ \mathbf{e}_{K-L}\right]$ and a signal subspace, respectively. The steering vector and the noise subspace $\mathbf{E}_N$ are orthogonal, and the spectrum function is as follow:

$$P\left(v_{t_0}\right) = \frac{1}{\mathbf{s}^{\mathrm{H}}\left(v_{t_0}\right)\mathbf{E}_N\mathbf{E}_N^{\mathrm{H}}\mathbf{s}\left(v_{t_0}\right)} \tag{11}$$

In which sharp peaks occur at the path change velocity of the signals.

After the above process, we could use Eq. (11) to calculate the path change velocity spectrum, Fig. 4(a) and (b) depict the path change velocity spectrum in TTW detection, respectively. In theory, TTW signal path only retains the dynamic path, and only one peak appears on the spectrum when there is an active human. The real peak of the spectrum does not appear when active human absence. In reality, TTW signal will be severely attenuated, which susceptible to noise, and it is difficult to completely remove all static paths and preserve the dynamic paths. Therefore, there are multiple peaks in Fig. 4, and we select the spectrum power of the largest peak to represent the value during this time. Figure 4(b) shows that there is no active human in the TTW detection, and the path change speed and its corresponding spectrum power may still have real peaks. Considering the above situation, it is difficult to directly detect active human using spectrum power estimated from TTW signal.

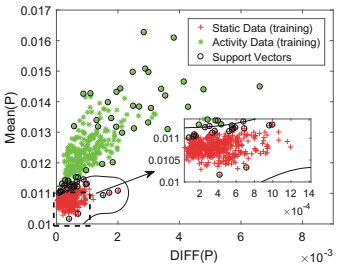

Fig. 6. The feature distribution of activity data and static data in TTW scenario.

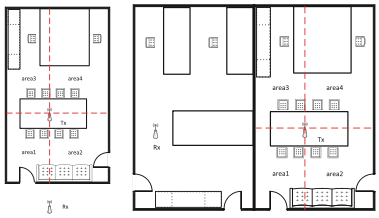

(a) Meeting room (b) Office room

Fig. 7. Experiment testbed.

Feature Extraction. As shown in Fig. 5(a), the TTW signal is attenuated the signal so that the static data is similar to the walk data, and the spectrum power estimated by the static data and the activity data is similar. Since it is difficult to directly use the estimated spectrum power, further feature extraction is required. Although the estimated spectrum power is similar, it can still be roughly divided into two parts. In this section, we calculate two characteristics of a period of data, one of which is the mean of the power spectrum power for a period of time $Mean\,(P) = \frac{1}{W} \sum_{w \in W} P\,(v_w)$, and the other is the mean of the first-order difference $DIFF\,(P)$:

$$DIFF\,(P) = \frac{1}{W-1} \sum_{w=1}^{W-1} |P\,(v_w) - P\,(v_{w+1})| \tag{12}$$

where W is the length of time. We use the sliding window method to calculate the mean and the mean of the first-order difference of the spectrum power. As shown in Fig. 5(b) and (c), the degree of discrimination between the two parts is improved.

To illustrate the reliability of the selected features, we conduct the SVM [13] based classification on training data, in which the kernel function is "rbf". As shown in Fig. 6, the training data can be used for obtaining an effective classifier.

4 Experiment and Evaluation

In this section, we first detail present the experiment settings and methodology. Then, we evaluate the performance of T-HuDe.

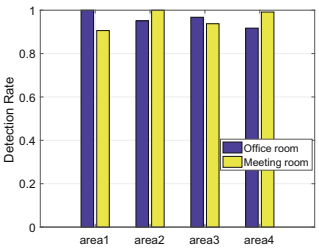

(a) TP rate in different scenarios

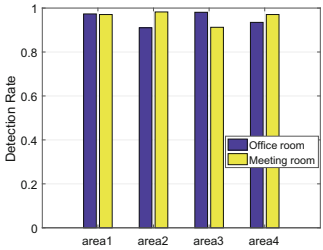

(b) TN rate in different scenarios

Fig. 8. Detection rate in different scenarios.

4.1 Experiment Methodology

To evaluate the performance of T-HuDe, we conduct experiments on the mini PC, which is equipped with Intel 5300 WiFi NIC and Ubuntu 10.04 Operating System (OS). CSI measurements are made for each packet using the Linux CSI tool [16]. The mini PC with one antenna is the transmitter, which operates in IEEE 802.11n AP mode at 5.745 GHz with 40 MHz bandwidth, and the mini PC with three antennas is the receiver, which collects 200 packets per second. We collect data in testbed as shown in Fig. 7. The testbed consists of two scenarios, meeting room and office room. In the meeting room scene, one of the AP is placed outside the room, and in the office room scene, the AP is placed in a different room, and all the walls are cement walls. The placement height of AP in all of these scenes are set to 1.1 m.

To test the impact of different areas on the detection rate, we divide the Tx room into 4 areas. The collected data includes two categories: (1) static data: there is no active human in the current environment; (2) activity data: there is an active human in the current environment, and the active human moving around in 4 areas, respectively.

4.2 Performance Evaluation

Evaluation Metric. To evaluate the performance of the T-HuDe system. We use the following two metrics.

- True Positive (TP) Rate: TP rate is the probability that an active human is correctly detected.
- True Negative (TN) Rate: TN rate is the probability that the static environment is correctly detected.

Overall Performance. We first depict TP rate and TN rate of systems working in different experimental cases. To evaluate the overall performance of T-HuDe, we calculate the spectrum power of the Doppler frequency shift with a window size of 0.5 s and calculate the eigenvalues using a parameter setting with a sliding

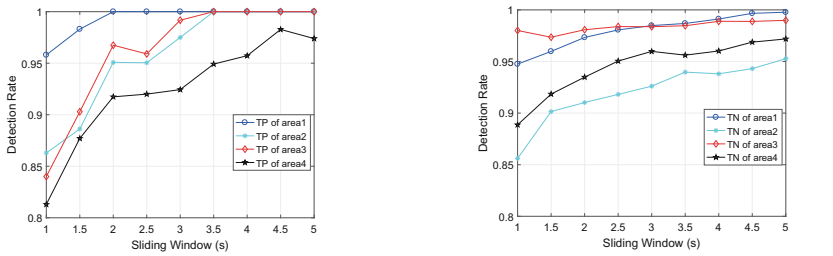

(a) Impact of sliding window on TP rate (b) Impact of sliding window on TN rate

Fig. 9. Impact of sliding window on detection rate.

window size of 2 s. Figure 8 presents results of four different test areas measured at different places, and shows that the system achieves excellent performance, the TP is higher than 93% in most areas. To make it clear, we compare the static data with the activity data of different areas respectively, and calculate the TN rate of different areas. As shown in Fig. 8(b), in most areas, the TN rate is also higher than 93%. However, the system has different detection rate in different areas, and the detection rate of each area is different. For office room scenarios, area1 and area3 have higher detection rate, and area2 and area4 have lower detection rate. For meeting room scenarios, area1 and area2 have higher detection rate and area3 has lower detection rate. In the higher detection rate areas, the active person is more likely to influence TTW signal, thus having a higher successful detection rate.

Impact of Sliding Window Size. We analyze the effect of sliding window size on TP and TN in different experimental areas. Generally, the detection rates of TP and TN rise as the sliding window size increases. Figure 9 illustrates this conjecture well, with the increase of the size of the sliding window, the detection rate of the system has increased. A reasonable explanation is that the influence of active human motion would be more probably captured when increasing the window size. In Fig. 9(a), the TP rate of most areas is maintained above 95% when the sliding window size exceeds 2.5 s, while the TP tends to be stable when the sliding window is increased to a certain size. When the sliding window size is less than 2 s, the performance of the system is less satisfied, mainly because the sampling time is too short to catch noticeable human movement. The same situation also occurs in Fig. 9(b). It is worth noting that the TP and TN detection rate of area1 are greater than 95% regardless of the sliding window size. The main reason is that area1 is the most sensitive area, and it is easy to detect the motion of the active human.

Compare Other Technologies. To verify the performance of the system, we compare T-HuDe with other systems. To be more specific, we compare T-HuDe with R-TTWD [9], which designed for the TTW human detection with

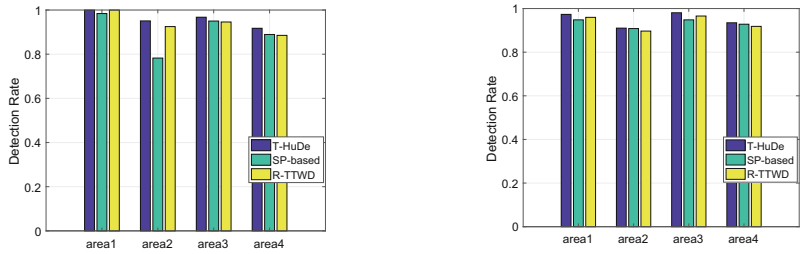

(a) TP rate in different system (b) TN rate in different system

Fig. 10. Detection rate in different system.

commodity devices, and relies on amplitude-based features for human detection. To calculate the features, the R-TTWD [9] applies wavelet denoising on the CSI, and performs a Principal Component Analysis (PCA) [17], and then calculates the mean of the first-order difference of the principal components. For fair comparison, we use the antenna selection strategy to select the appropriate single antenna data, and use two eigenvalues in R-TTWD [9], including the mean of the first-order difference of the second principal component and the third principal component. Besides, we also test the detection rate using a fixed threshold based approach to spectrum power, which denoted as "SP-based" in Fig. 10.

Figure 10 shows TP rate and TN rate of systems working in TTW scenarios, and the three detection systems show different detection rate in different areas, which means that the areas have different impact on performance. T-HuDe achieves TP rate and TN above 93% in most areas. SP-based also achieves a good detection rate in most areas, but T-HuDe outperformes SP-based at most places, and SP-based is susceptible to environmental influences, such as TP rate in area 2. In addition, the performance of R-TTWD is acceptable, but it is less satisfied compared to T-HuDe.

5 Conclusion

In this paper, we present an accurate and robustness TTW active human detection system with commodity WiFi devices. Since the different performance of different antennas, we use the antenna selection strategy to select the appropriate antenna and use a bandpass filter to filter out the noise signal. Then, we introduce Doppler-MUSIC to estimate the spectrum power corresponding to the Doppler velocity. Afterwards, we calculate the mean and the mean of the first-order difference of the spectrum power over time to achieve active human detection in TTW. We prototype T-HuDe in two indoor environments, and the experiment results show that the TP rate and TN rate of the system are better than 93% in most areas.

References

1. Xiao, J.: Enhancing WLAN-based indoor localization with channel state information. Hong Kong University of Science and Technology, Hong Kong (2014)
2. Li, X., Li, S., Zhang, D., Xiong, J., Wang, Y., Mei, H.: Dynamic-music: accurate device-free indoor localization. In: Proceedings of the 2016 ACM International Joint Conference on Pervasive and Ubiquitous Computing, pp. 196–207. ACM (2016)
3. Duan, S., Yu, T., He, J.: WiDriver: driver activity recognition system based on WiFi CSI. Int. J. Wirel. Inf. Networks **25**(2), 146–156 (2018)
4. Wang, H., Zhang, D., Wang, Y., Ma, J., Wang, Y., Li, S.: RT-fall: a real-time and contactless fall detection system with commodity wifi devices. IEEE Trans. Mob. Comput. **16**(2), 511–526 (2016)
5. Wang, Y., Wu, K., Ni, L.M.: WiFall: device-free fall detection by wireless networks. IEEE Trans. Mob. Comput. **16**(2), 581–594 (2016)
6. Wang, X., Yang, C., Mao, S.: PhaseBeat: exploiting CSI phase data for vital sign monitoring with commodity wifi devices. In: 2017 IEEE 37th International Conference on Distributed Computing Systems (ICDCS), pp. 1230–1239. IEEE (2017)
7. Liu, X., Cao, J., Tang, S., Wen, J., Guo, P.: Contactless respiration monitoring via off-the-shelf wifi devices. IEEE Trans. Mob. Comput. **15**(10), 2466–2479 (2015)
8. Youssef, M., Mah, M., Agrawala, A.: Challenges: device-free passive localization for wireless environments. In: Proceedings of the 13th Annual ACM International Conference on Mobile Computing and Networking, pp. 222–229. ACM (2007)
9. Zhu, H., Xiao, F., Sun, L., Wang, R., Yang, P.: R-TTWD: robust device-free through-the-wall detection of moving human with wifi. IEEE J. Sel. Areas Commun. **35**(5), 1090–1103 (2017)
10. Qian, K., Wu, C., Yang, Z., Liu, Y., Zhou, Z.: PADS: passive detection of moving targets with dynamic speed using PHY layer information. In: 2014 20th IEEE International Conference on Parallel and Distributed Systems (ICPADS), pp. 1–8. IEEE (2014)
11. Lv, J., Yang, W., Gong, L., Man, D., Du, X.: Robust WLAN-based indoor fine-grained intrusion detection. In: 2016 IEEE Global Communications Conference (GLOBECOM), pp. 1–6. IEEE (2016)
12. Li, X., et al.: IndoTrack: device-free indoor human tracking with commodity wi-fi. Proc. ACM Interact. Mob. Wearable Ubiquit. Technol. **1**(3), 72 (2017)
13. Boser, B.E., Guyon, I.M., Vapnik, V.N.: A training algorithm for optimal margin classifiers. In: Proceedings of the fifth Annual Workshop on Computational Learning Theory, pp. 144–152. ACM (1992)
14. Wang, W., Liu, A.X., Shahzad, M., Ling, K., Lu, S.: Understanding and modeling of wifi signal based human activity recognition. In: Proceedings of the 21st Annual International Conference on Mobile Computing and Networking, pp. 65–76. ACM (2015)
15. Qian, K., Wu, C., Zhou, Z., Zheng, Y., Yang, Z., Liu, Y.: Inferring motion direction using commodity wi-fi for interactive exergames. In: Proceedings of the 2017 CHI Conference on Human Factors in Computing Systems, pp. 1961–1972. ACM (2017)
16. Li, Z., Tian, Z., Zhou, M., Jin, Y.: Wi-vision: an accurate and robust LOS/NLOS identification system using Hopkins statistic. In: GLOBECOM 2017–2017 IEEE Global Communications Conference, pp. 1–6. IEEE (2017)
17. Abdi, H., Williams, L.J.: Principal component analysis. Wiley Interdisc. Rev.: Computat. Stat. **2**(4), 433–459 (2010)